Contents lists available at ScienceDirect

Digital Signal Processing

journal homepage: www.elsevier.com/locate/dsp

Decorrelation spectrum sensing model with structural information learning

Haihui Xie [a,b], Shuwu Chen [a,b,*], Zhaogang Shu [a,b], Fangqing Tan [a,b]

[a] College of Computer and Information Sciences, Fujian Agriculture and Forestry University, 350002, Fuzhou, China
[b] School Of Information and Communication, Guilin University Of Electronic Technology, 541004, Guilin, China

ARTICLE INFO

Keywords:
Signal reconstruction
Spark
Structural information learning
Wideband spectrum sensing

ABSTRACT

In cognitive radio, spectrum sensing is promising to detect the spectrum holes. To recover the spectrum from sub-Nyquist samples efficiently, this paper proposes a novel spectrum reconstruction model with structural information matrix. In particular, we first design a sparsity bound learning algorithm to degrade the influence of correlated information. Then, we employ a spark information to learn the sparse structure of spectrum signals efficiently. Last, we develop an adaptively-regularized iterative reweighted least squares (AR-IRLS) algorithm to solve the large-scale optimization problem. Extensive simulation results demonstrate the effectiveness of the proposed algorithm and evaluate its performance in practical spectrum sensing cases.

1. Introduction

With the explosive growth of Internet of Things devices, the demand for spectrum resources is rapidly increasing, exacerbating the issue of spectrum scarcity [1]. This problem is particularly pronounced in low and medium frequency bands that inherit good propagation characteristics. Cognitive radio is a promising paradigm for wireless communication to degrade the interference to primary users while opportunistically accessing spectrum holes. To detecting these spectrum holes efficiently, spectrum sensing is essential in cognitive radio networks [2,3].

Wideband spectrum sensing has garnered significant attention due to its critical applications in cognitive radios. In these applications, it is essential to identify the frequency locations of multiple signals distributed across a wide frequency band. This task leverages the inherent sparsity of signals in the frequency domain, formulating wideband spectrum sensing as a sparse signal recovery problem [4]. For spectrum sensing, the primary objective is detection, and reconstructing the original signal is often unnecessary.

1.1. Related works and motivation

In compressive spectrum sensing (CSS) architectures, multirate sampling [5,6], multicoset sampling [7,8], modulated wideband converter [9,10] utilize the sparsity prior structure of the signals to solve the spectrum sensing problems. The works [5,6] designed multirate sampling architectures for sparse array signal acquisition. However, their performance was limited by time synchronization accuracy. The works [7,8] developed multicoset sampling schemes to obtain high-speed and high-precision performance. However, these schemes suffered from multichannel mismatch, and then failed to obtain a high-significant. The modulated wideband converter architectures [9,10] relied on sub-Nyquist sampling to achieve the full-band signal has high computational and complexity sensing with the low-speed circuits. Nevertheless, these CSS-based architectures have high computational and complexity and require high signal-to-noise-ratio (SNR) for the prior information acquisition. Meanwhile, they potentially lead to a miss of some weak signals due to the folded noise and harmonics.

To overcome the drawback of CSS-based methods, the works [11–16] also have reconstructed compressive covariance sensing (CCS) architectures. The works [11,12] designed the covariance matrix structures to effectively suppress the folded noise and harmonics, and support the low-SNR conditions for the wideband spectrum sensing. The works [13,14] focused on the CCS-based wideband power spectrum sensing, divided into the time-domain [13] and the frequency domain approaches [14]. The works [15,16] have utilized the covariance matric and sparse regularization terms to constrain the signal structure to solve the power spectrum blind sampling problem. However, the sensing performance of most existing CCS excessively relies on the prior information such as spectrum sparsity or noise variance. It is hard to work effectively even in the absence of such information.

To detect as much spectrum opportunities as possible from wide frequency bands, various optimization algorithms have been developed for the wideband spectrum sensing, including greedy and iterative algorithms. The greedy algorithms, e.g., orthogonal matching pursuit (OMP) [17,18], simultaneous orthogonal matching pursuit (SOMP) [19,20] and

* Corresponding author.
E-mail addresses: xiehh@fafu.edu.cn (H. Xie), chenshuwu@fafu.edu.cn (S. Chen), zgshu@fafu.edu.cn (Z. Shu), tfqing@guet.edu.cn (F. Tan).

https://doi.org/10.1016/j.dsp.2025.105759

Table 1
Comparison of existing and proposed schemes.

Modulation	Work	Decorrelation	Sparsity Requirement	Computational Complexity	MSE	Convergence Speed	Low-SNR
CSS-based	[5,6]	✗	Prior-based	+ + +	+ + +	+	✗
	[7,8]	✗	Prior-based	+ + +	+ + +	+	✗
	[9,10]	✗	Prior-based	+ + +	+ + +	+	✗
CCS-based	[11,12]	✗	✗	+ + +	+ +	+	✓
	[13,14]	✗	✗	+ + +	+ +	+	✓
	[15,16]	✗	✗	+ + +	+ +	+	✓
	[17–25]	✗	✗	+ +	+ +	+ +	✓
	Proposed	✓	**Learning-based**	+ +	+	+ + +	✓

The symbol "+" means low, "+ +" means moderate, "+ + +" means high. The symbol "✓" means functionality supported, "✗" means functionality not supported.

other variant greedy algorithms [21], exhibited satisfactory sensing performance with low complexity. On the other hand, the works have proposed various iterative reweighted least squares (IRLS) algorithms with regression regulation to compel spectrum recovery performance with few measurements [22–24]. Moreover, the work [25] also designed an adaptively-regularized IRLS (AR-IRLS) algorithm, improving the sensing efficiency and recovery performance.

However, those greedy selection algorithms require the spectrum prior sparsity or mutual incoherence information [17–21]. The sparsity level and measurements incoherence of spectrum sensing are hard to be obtained, therefore this limits the applicability of greedy algorithms. In contrast, the conventional IRLS algorithms contains an inverse problem of the system matrix at each iteration, and cannot meet the real-time requirement due to its high computational complexity [22–25]. Moreover, these IRLS algorithms also fail to fully recover the signal sparsity, and yield a descent direction of optimization objectives. The estimation of sparsity level is hard for time-varying spectrum channels, leading to high sensing errors and substantial computational demands.

To make IRLS algorithms suitable for spectrum sensing, we design a novel structural information matrix that enables the signal recovery process to learn the structural information of spectrum sensing models, significantly enhancing the accuracy and robustness of signal reconstruction. To further improve sparsity degree and effective noise reduction, we introduce an AR-IRLS algorithm with sparsity-bound learning. Compared with AR-IRLS and IRLS algorithms, our proposed algorithm dynamically learns sparsity information and utilize the Spark to mitigate the influence of signal correlation at each iteration. This also ensures stable convergence as the number of iterations increases. Additionally, we apply the proposed algorithm to two typical spectrum sensing problems involving widesense stationary multi-band signals. Numerical and experimental results demonstrate that the proposed algorithm achieves superior performance given higher sparsity and fewer measurements conditions, in terms of both accuracy and computational efficiency. In brevity, Table 1 compares the existing and proposed schemes.

1.2. Summary of main results

In this paper, we first propose a spectrum sensing model with structural information matrix. Then, we formulate an optimization problem, and provide a closed-form solution. Third, we develop an adaptive structure-promoting matrix, agreeing with structural information and Spark of sensing matrix, and then design an iterative algorithm to reduce complexity. Last, we demonstrate the spectrum sensing simulation for different settings and algorithms. In summary, the mainly three contributions of this paper are as follows.

1) The spectrum sensing model with structural information matrix is proposed. This matrix reflects the structure information of transformation, which enables the signal recovery process to learn these information and achieve a high precision by constructing the regularization. Moreover, the proposed model demonstrates robustness to dynamic noise variations.
2) The structural information matrix is designed by sparsity bound learning and Spark. Specifically, this structural matrix enables seek the sparser representation in the signal reconstruction process. Moreover, the proposed adaptively reduces signal correlation, and minimizes redundant information computation.
3) The accelerated IRLS algorithm is developed to make the IRLS algorithm more efficient for a large-scale matrix. Specifically, an outer-product approximation is designed to develop a computationally efficient procedure for approximating the inverse process. Moreover, the binary structure of weights also minimizes the flops, enhancing the computational efficiency.

1.3. Organization

The rest of this paper is organized as follows. In Section 2, we propose a spectrum sensing model with structural information matrix. In Section 3, we formulate an optimization problem, and then provide a closed-form solution. In Section 4, we develop an adaptive structure-promoting matrix and design an iterative algorithm. In Section 5, we demonstrate the spectrum sensing simulation for different settings. In Section 6, we briefly conclude with a discussion.

Notations: The following notations are used throughout this paper. In the sequel, vectors are denoted by lowercase boldface, matrices by uppercase boldface, and the transpose by the superscript $(\cdot)^T$. In particular, symbol $\boldsymbol{\Phi}$ denotes the sampling matrix, $\boldsymbol{A}$ denotes the sensing matrix, $\boldsymbol{B}$ denotes the structure-promoting matrix, $\boldsymbol{W}$ denotes the diagonal weight matrix. The $x(t)$ denotes the continuous-time wideband signal, $\boldsymbol{\alpha}$ denotes the relative Nyquist samples, $\boldsymbol{x}$ denotes the sparse representation in the frequency domain. The $\mathcal{S}$ denotes the structural information, $\mathcal{S}^c$ denotes the complementary of the bound $\mathcal{S}$. Notation $[\cdot]_t$ represents the relative variable at the t^{th} iteration. Notation $\mathcal{R}(\cdot)$ denotes the range space, $\mathcal{N}(\cdot)$ denotes the null space. Notation $\mathrm{supp}(\cdot)$ denotes the set of the indexes of the non-zero values in the relative vector.

2. Spectrum sensing model with structural information

In this section, we first propose a spectrum reconstruction model with structural information matrix. Then, we also derive a similar structure in power spectrum reconstruction model.

2.1. Spectrum reconstruction model

We first analyze the spectrum reconstruction. Let $x(t)$ be a continuous-time signal defined over the interval $[0, T)$. Its Fourier series representation is given by

$$x(t) = \frac{1}{\sqrt{T}} \sum_{k=-Q/2}^{Q/2} a_k e^{j\frac{2\pi k}{T}t}, \quad t \in [0, T),$$

where $Q/(2T)$ is the maximal possible frequency in $x(t)$. For this model we consider the Nyquist samples of $x(t)$, defined as

$$\alpha(n) = x(nT_s), \quad 0 \le n < N,$$

where $T_s = T/(Q+1)$ denotes the sampling period. Typically, $N \triangleq T/T_s = Q+1$ denotes the number of the Nyquist samples [26]. For spectrum reconstruction and power spectrum reconstruction model, we consider the relative digital model at the frequency domain.

Let $\boldsymbol{F} \in \mathbb{R}^{N\times N}$ be the discrete Fourier transmission (DFT) matrix and $\boldsymbol{c}$ as the DFT coefficients of $\boldsymbol{\alpha}$, then we get

$$\boldsymbol{c} \triangleq \boldsymbol{B}_c^H \boldsymbol{F}\boldsymbol{\alpha} \tag{1}$$

where $\boldsymbol{B}_c \in \mathbb{R}^{N\times N^2}$ is a selection matrix with a full row rank for a sensing system of only zero and one element. Here, $\boldsymbol{B}_c$ maps the information of $\boldsymbol{c}$ to another space that reflects the structure information of $\boldsymbol{C}_c$ while preserving the computational results. It reflects the structural information of the target vector. Moreover, we also define the autocorrelation matrix of $\boldsymbol{c}$ as

$$\boldsymbol{C}_c \triangleq \mathbb{E}\left(\boldsymbol{c}\boldsymbol{c}^H\right). \tag{2}$$

Consequently, our objective is to recover the autocorrelation matrix $\boldsymbol{C}_c$. Since $\boldsymbol{\alpha}$ is a widesense stationary signal, the cross-correlation terms need satisfy

$$\mathbb{E}\left(\boldsymbol{c}(k)\boldsymbol{c}^*(l)\right) = 0, \text{ for } k \neq l, \quad \boldsymbol{C}_c(i,i) = \mathbb{E}\left[|\boldsymbol{c}(i)|^2\right]. \tag{3}$$

Let $\boldsymbol{z} \in \mathbb{R}^M$ denote the sub-Nyquist samples in terms of the Nyquist samples $\boldsymbol{\alpha}$ as

$$\boldsymbol{z} = \boldsymbol{\Phi}\boldsymbol{\alpha}, \tag{4}$$

where $\boldsymbol{\Phi} \in \{0,1\}^{M\times N^2}$ is defined as a selection matrix in the multicoset sampling scheme [15,27]. Combining DFT with (4), we obtain

$$\boldsymbol{z} = \frac{1}{N}\boldsymbol{\Phi}\boldsymbol{F}^H\boldsymbol{B}_c\boldsymbol{c} = \boldsymbol{G}\boldsymbol{B}_c\boldsymbol{c}, \tag{5}$$

where $\boldsymbol{G} \triangleq \frac{1}{N}\boldsymbol{\Phi}\boldsymbol{F}^H$. Combining the sparsity of the DFT coefficients $\boldsymbol{c}$ with (5), we can formulate the spectrum sensing problem from the measurement $\boldsymbol{z}$, namely,

$$\begin{aligned} \mathcal{P}1: &\min_{\boldsymbol{c}} \|\boldsymbol{B}_c\boldsymbol{c}\|_0 \\ &\text{s.t. } \boldsymbol{z} = \boldsymbol{G}\boldsymbol{c}. \end{aligned}$$

2.2. Power spectrum reconstruction model

Next, we also design the power spectrum reconstruction model with resembling structures of $\mathcal{P}1$. Let $\boldsymbol{C}_z = \mathbb{E}\left[\boldsymbol{z}\boldsymbol{z}^H\right]$ be an autocorrelation matrix of sub-Nyquist samples, we have

$$\boldsymbol{C}_z = \boldsymbol{G}\boldsymbol{C}_c\boldsymbol{G}^H, \tag{7}$$

where (7) is derived from (2) and (5). Taking the vectorization of (7), we have

$$\boldsymbol{r}_z = (\overline{\boldsymbol{G}} \otimes \boldsymbol{G})\text{vec}\left(\boldsymbol{C}_c\right) = (\overline{\boldsymbol{G}} \otimes \boldsymbol{G})\boldsymbol{B}_r\boldsymbol{r}_c = \boldsymbol{A}\boldsymbol{r}_c, \tag{8}$$

where $\boldsymbol{B}_r \in \mathbb{R}^{N^2\times N}$ is also defined as a selection matrix with a full column rank, $\otimes$ denotes Kronecker product, $\overline{\boldsymbol{G}}$ denotes the conjugate matrix of $\boldsymbol{G}$, $\boldsymbol{A} \triangleq (\overline{\boldsymbol{G}} \otimes \boldsymbol{G})\boldsymbol{B}_r$ is a compressive sensing matrix of size $M^2 \times N$ and $\boldsymbol{r}_c$ is a vector of size N that contains the diagonal elements of $\boldsymbol{C}_c$, namely, $\boldsymbol{r}_c(i) = \boldsymbol{C}_c(i,i)$, $1 \le i \le N$. Obviously, $\boldsymbol{B}_r$ also reflects the structure information of $\boldsymbol{C}_c$. Similar to $\mathcal{P}1$, we also formulate the power spectrum sensing problem, namely,

$$\begin{aligned} \mathcal{P}2: &\min_{\boldsymbol{r}_c} \|\boldsymbol{B}_r\boldsymbol{r}_c\|_0 \\ &\text{s.t. } \boldsymbol{r}_z = \boldsymbol{A}\boldsymbol{r}_c. \end{aligned}$$

Combining $\mathcal{P}1$ with $\mathcal{P}2$, we design a structural information matrix $\{\boldsymbol{B}_c, \boldsymbol{B}_r\}$ in spectrum sensing model, which enables the signal recovery process to learn the structural information.

$$\mathcal{P}3: \min_{\boldsymbol{x}} \|\boldsymbol{B}_t\boldsymbol{x}\|_0 \tag{10a}$$

$$\text{s.t. } \boldsymbol{y} = \boldsymbol{A}\boldsymbol{x}. \tag{10b}$$

where $\boldsymbol{x} \in \mathbb{R}^N$, $\boldsymbol{y} \in \mathbb{R}^M$, $\boldsymbol{A} \in \mathbb{R}^{M\times N}$ represent the recovered signal, the observed signal, and the compressive sensing matrix, respectively. $\boldsymbol{B}_t \in \mathbb{R}^{t\times N}$ is a structure-promoting matrix [28] that moves some components of the optimization solution $\boldsymbol{x}$ toward zero. Specifically, as the number of iterations increases, the rows of the structure-promoting matrix are developed to incorporate the structural information, and feeds it back into the signal recovery, thereby improving the recovered signal's compliance with the spectrum sensing.

Remark 1 (Detection Threshold)**.** When the recovered signal $\boldsymbol{x}^*$ is obtained by $\mathcal{P}3$, combining the energy density of $\boldsymbol{x}^*$ with a detection threshold ϕ_d can determine the spectrum occupancy, given by [12,25]

$$\phi_d = \sigma_n^2\left(1 + \frac{\mathrm{Q}^{-1}(P_\mathrm{f})}{\sqrt{N/2}}\right),$$

where σ_n^2, P_f, Q represent the noise variance, the target probability of false alarm, and Q function, respectively. If the energy of the reconstructed signal is higher than ϕ_d, the channel is occupied. Otherwise, the corresponding channel is vacant.

Compared with [4,15,16,18], $\mathcal{P}3$ is adaptive to real-time transformation information, and enables more rational signal recovery based on such information, resulting in a high precision in signal reconstruction. To solve $\mathcal{P}3$ efficiently, we propose an adaptive algorithm that learns the underlying structures, ensuring efficient and accurate signal recovery.

3. Adaptively spectrum sensing model

In this section, we formulate an optimization problem, and then provide a closed-form solution. There exists a traditional model [23] to solve the sparse linear problem $\mathcal{P}3$ as follows

$$\mathcal{P}4: \min_{\boldsymbol{x}}\left\{\frac{1}{2}\|\boldsymbol{A}\boldsymbol{x} - \boldsymbol{y}\|_2^2 + \lambda\|\boldsymbol{B}_t\boldsymbol{x}\|_p\right\},$$

where λ is a nonnegative real number, and $\|\cdot\|_p$ means ℓ_p-norm ($0 < p \le 1$).

Since the optimization problem $\mathcal{P}4$ is a non-convex function, the following smooth function $J_\epsilon(\boldsymbol{x})$ [23] is used to approximate it, namely,

$$J_\epsilon(\boldsymbol{x}) = \frac{1}{2}\|\boldsymbol{A}\boldsymbol{x} - \boldsymbol{y}\|_2^2 + \lambda\sum_i^t \varphi(\boldsymbol{b}_i^T\boldsymbol{x}), \tag{11}$$

where each vector $\boldsymbol{b}_i^T$ is the i^{th} row of $\boldsymbol{B}_t$ and the function $\varphi(v)$ is given by

$$\varphi(v) = \begin{cases} \frac{p}{2}\epsilon^{p-2}v^2 + \frac{2-p}{2}\epsilon^p, & \text{if } |v| < \epsilon, \\ |v|^p, & \text{otherwise } |v| \ge \epsilon. \end{cases} \tag{12}$$

The function (11) is strictly convex and its minimizer is given by

$$\boldsymbol{x}_{t+1} = (\boldsymbol{A}^T\boldsymbol{A} + \boldsymbol{B}_t^T\boldsymbol{W}_t\boldsymbol{B}_t)^{-1}\boldsymbol{A}^T\boldsymbol{y}, \tag{13}$$

where $\boldsymbol{W}_t = \text{diag}(\boldsymbol{w}_{\boldsymbol{x}_t})$, $\boldsymbol{w}_{\boldsymbol{x}_t} \triangleq \left[\omega_1, \omega_2, \ldots, \omega_t\right]$ and $\boldsymbol{b}_i^T$ $(i \in \{1, 2, \ldots, t\})$ is the i^{th} row of $\boldsymbol{B}_t$. Specifically, each weight of $\boldsymbol{w}_{\boldsymbol{x}_t}$ is defined as

$$\omega_i = \lambda\min(p\epsilon^{p-2}, \ p|\boldsymbol{b}_i^T\boldsymbol{x}_t|^{p-2}). \tag{14}$$

From the necessary condition $\mathcal{N}(\boldsymbol{A})\bigcap\mathcal{N}(\boldsymbol{B}_t) = \{\boldsymbol{0}\}$, we expect that $\mathcal{N}(\boldsymbol{A})$ is enough close to the subspace of $\lim_{t\to\infty}\mathcal{R}(\boldsymbol{B}_t^T)$ as the estimator $\boldsymbol{x}_t$ gets more accurate, and the problem $\mathcal{P}4$ can converge to the sparser optimization solution [22,29]. However, as the number of iterations increases, the dimension of $\boldsymbol{B}_t$ grows rapidly, resulting in high computational complexity of (13). It fails to meet the real-time requirements of spectrum sensing systems. Therefore, we propose a structural information learning algorithm to construct $\boldsymbol{B}_t$ in the next section.

4. Upper bound for sparsity learning algorithm

In this section, we propose an algorithm to seek a better approximation of the matrix $\boldsymbol{B}_t$ in the problem $\mathcal{P}4$ for structural information learning, and then derive a sequential procedure for solving the matrix inverse problem (13).

4.1. Sparsity bound for ℓ_1-norm optimization

For two any strictly feasible representations $\boldsymbol{x}_0$, $\boldsymbol{x}_1$ ($\boldsymbol{y} = \boldsymbol{A}\boldsymbol{x}_0 + \boldsymbol{n} = \boldsymbol{A}\boldsymbol{x}_1 + \boldsymbol{n}$), suppose $\|\boldsymbol{x}_0\|_0 \geq \|\boldsymbol{x}_1\|_0$ and $\mathrm{supp}(\boldsymbol{x}_1) \subseteq \mathrm{supp}(\boldsymbol{x}_0)$. To show that ℓ_1-norm optimization problem can obtain the sparser representation $\boldsymbol{x}_0$, we need to show that $\|\boldsymbol{x}_0\|_1 \geq \|\boldsymbol{x}_1\|_1$. So ℓ_1-norm optimization problem [22] can be obtained by

$$\begin{aligned}\mathcal{P}5 :\ & \min\ \|\boldsymbol{x}_0\|_1 - \|\boldsymbol{x}_1\|_1 \\ & \text{s.t. } \boldsymbol{y} = \boldsymbol{A}\boldsymbol{x}_0 + \boldsymbol{n} = \boldsymbol{A}\boldsymbol{x}_1 + \boldsymbol{n}, \\ & \qquad \|\boldsymbol{x}_0\|_1 \geq \|\boldsymbol{x}_1\|_1.\end{aligned}$$

In order to study the behavior of $\mathcal{P}5$, we define the residual vector as $\boldsymbol{\Delta} \triangleq \boldsymbol{x}_0 - \boldsymbol{x}_1$. And the problem $\mathcal{P}5$ can be approximated as

$$\begin{aligned}\mathcal{P}6 :\ & \max_{\mathcal{S}} \sum_{k\in\mathcal{S}} |\boldsymbol{\Delta}(k)| \\ & \text{s.t. } \boldsymbol{A}\boldsymbol{\Delta} = \boldsymbol{0}, \\ & \qquad \sum_{k\in\mathcal{S}} |\boldsymbol{\Delta}(k)| < \frac{1}{2}\|\boldsymbol{\Delta}\|_1, \\ & \qquad \mathrm{supp}(\boldsymbol{x}_1) \subseteq \mathcal{S} \subseteq \mathrm{supp}(\boldsymbol{x}_0).\end{aligned}$$

The transformation process is derived from Appendix A.

Above all, the optimization solution of the problem $\mathcal{P}6$ is closely related to one of the problem $\mathcal{P}5$ [22]. It can be seen that if $\mathrm{supp}(\boldsymbol{x}_1) \subseteq \mathcal{S}$ and $\left(\max_{\mathcal{S}} \sum_{k\in\mathcal{S}} |\boldsymbol{\Delta}(k)|\right) < 1/2\|\boldsymbol{\Delta}\|_1$, then $\boldsymbol{x}_1$ is the unique sparsest solution of ℓ_1-norm problem from $\boldsymbol{y} = \boldsymbol{A}\boldsymbol{x}_1 + \boldsymbol{n}$. It is straightforward that if $\left(\max_{\mathcal{S}} \sum_{k\in\mathcal{S}} |\boldsymbol{\Delta}(k)|\right) \geq 1/2\|\boldsymbol{\Delta}\|_1$, $\boldsymbol{x}_1$ is not the unique sparsest solution of ℓ_1-norm problem.

Lemma 1. *Suppose there exists a sequence of strictly feasible representations* $\left\{\boldsymbol{x}_1, \boldsymbol{x}_2, \dots, \boldsymbol{x}_\tau, \dots \,\middle|\, \boldsymbol{y} = \boldsymbol{A}\boldsymbol{x}_i + \boldsymbol{n}\ (i = 1, 2, \dots, \tau, \dots)\right\}$ *and they satisfy the following conditions,*

$$\mathrm{supp}\{\boldsymbol{x}_1\} \supseteq \mathrm{supp}\{\boldsymbol{x}_2\} \cdots \supseteq \mathrm{supp}\{\boldsymbol{x}_\tau\} \dots,$$

then we can obtain the following properties

$$\begin{aligned}&\mathrm{supp}\{\boldsymbol{x}_i\} \supseteq \mathcal{S}_i \supseteq \mathrm{supp}\{\boldsymbol{x}_{i+1}\}, \quad (i = 1, \dots, \tau - 1), \\ &\mathcal{S}_1 \supseteq \mathcal{S}_2 \cdots \supseteq \mathcal{S}_\tau = \cdots = \mathcal{S}^*,\end{aligned}$$

where $\mathcal{S}_i$ denotes the structural information from the optimization problem $\mathcal{P}6$ given two representations $\boldsymbol{x}_i$, $\boldsymbol{x}_{i+1}$. When $\mathrm{supp}(\boldsymbol{x}_i) = \mathrm{supp}(\boldsymbol{x}_{i+1})$, the structural information $\mathcal{S}_i = \mathrm{supp}(\boldsymbol{x}_i) = \mathrm{supp}(\boldsymbol{x}_{i+1}) = \mathcal{S}^*$.

Proof. The proof is referred to Appendix A. □

Following the above analysis on the structural information $\mathcal{S}_t$ of optimization solution, we propose the binary vector $\boldsymbol{s}_t^T$ as a new row of $\boldsymbol{B}_t$ at t^{th} iteration, namely,

$$\boldsymbol{B}_t^T \triangleq \left[\boldsymbol{s}_1, \boldsymbol{s}_2, \dots, \boldsymbol{s}_t\right] = \left[\boldsymbol{B}_{t-1}^T, \boldsymbol{s}_t\right],$$

where $|\boldsymbol{s}_t| \triangleq \boldsymbol{1} - \boldsymbol{1}_{\mathcal{S}_t}$ corresponds to the structural information vector associated with $\boldsymbol{x}_t$ and $\boldsymbol{1}$ is a vector filled with ones, $\boldsymbol{1}_{\mathcal{S}_t}$ is an indicator, where $\boldsymbol{1}_{\mathcal{S}_t}(i) = 1$ if i is in the structural information $\mathcal{S}_t$ of $\boldsymbol{x}_t$ and zero elsewhere. Additionally, to guarantee performance and that the sign does not affect the optimization process, $\mathrm{sign}(\boldsymbol{s}_t) = \mathrm{sign}(\boldsymbol{x}_t)$ can be satisfied. So it suffices to obtain a binary vector $\boldsymbol{s}_t$ such that

$$\boldsymbol{s}_t(k) = \begin{cases}\mathrm{sign}\left(\boldsymbol{x}_t(k)\right), & k \in \mathcal{S}_t^c \\ 0, & k \in \mathcal{S}_t\end{cases}. \tag{16}$$

Substituting (16) into (14), we have

$$\omega_i = \lambda \min(p\varepsilon^{p-2},\ p|\boldsymbol{s}_i^T\boldsymbol{x}_i|^{p-2})\ (i \in \{1, 2, \dots, t\}). \tag{17}$$

4.2. Spark information

Assume there exist two different suitable representations $\boldsymbol{x}_0$, $\boldsymbol{x}_1$ ($\boldsymbol{x}_0 \neq \boldsymbol{x}_1$) for an incoming signal vector $\boldsymbol{y}$ by using the sensing matrix $\boldsymbol{A}$, namely,

$$\boldsymbol{y} = \boldsymbol{A}\boldsymbol{x}_1 + \boldsymbol{n} = \boldsymbol{A}\boldsymbol{x}_0 + \boldsymbol{n}. \tag{18}$$

Thus we can conclude that the residual vector $\boldsymbol{\Delta} = \boldsymbol{x}_0 - \boldsymbol{x}_1$ must be in the null space $\mathcal{N}(\boldsymbol{A})$, and there exist a group of linearly-dependent columns of $\boldsymbol{A}$. To discuss the size of this group, the Spark is defined as the smallest number of columns from $\boldsymbol{A}$ that are linearly dependent [28]. In the following context, we define the Spark as $\sigma \triangleq \mathrm{Spark}(\boldsymbol{A})$.

To evaluate this Spark, we can bound the Spark solving ℓ_1-norm problem [22] as

$$\begin{aligned}\mathcal{P}7 :\ & \min\ \|\boldsymbol{\Delta}\|_1 \\ & \text{s.t. } \boldsymbol{A}\boldsymbol{\Delta} = \boldsymbol{0}, \\ & \qquad \boldsymbol{\Delta}(k) = 1.\end{aligned}$$

Denote the solution of the problem $\mathcal{P}7$ by $\boldsymbol{\Delta}^{*,k}$, so solving this Spark can be approximated by

$$\mathcal{P}8 :\ \min_{1\leq k\leq N} \|\boldsymbol{\Delta}^{*,k}\|_0.$$

In this numerical experiment, $\mathcal{P}7$ and $\mathcal{P}8$ can be solved by standard convex solvers, e.g., CVX [30]. This bound tends to be quite tight, and close to the true Spark.

We now use the Spark to bound the sparsity of nonunique representation [28]. Every nonuniqueness pair $(\boldsymbol{x}_0, \boldsymbol{x}_1)$ generates $\boldsymbol{\Delta}$ in the column null-space and

$$\boldsymbol{A}\boldsymbol{\Delta} = \boldsymbol{0} \Longrightarrow \|\boldsymbol{x}_0 - \boldsymbol{x}_1\|_0 = \|\boldsymbol{\Delta}\|_0 \geq \sigma.$$

According to the property of triangle inequality, we have

$$\sigma \leq \|\boldsymbol{x}_0 - \boldsymbol{x}_1\|_0 \leq \|\boldsymbol{x}_0\|_0 + \|\boldsymbol{x}_1\|_0. \tag{20}$$

From (20), we can see that if there exists a representation satisfying $\|\boldsymbol{x}_1\|_0 < \sigma/2$, then any other representation $\boldsymbol{x}_0$ must satisfy $\|\boldsymbol{x}_0\|_0 > \sigma/2$, implying that $\boldsymbol{x}_1$ is the sparsest representation.

Given the sparsity bound and spark information, we design an iterative algorithm to learn the sparse structure of spectrum signals. We first utilize a bisection method to solve $\mathcal{P}6$ efficiently, updating the structural information $\mathcal{S}$ of optimization signals. The basic idea of this algorithm is to find a upper bound $\mathcal{S}$ for structural information along with the signal reconstruction process. Since the objective in $\mathcal{P}6$ is the maximization of the term $\max_{\mathcal{S}} \sum_{k\in\mathcal{S}} |\boldsymbol{\Delta}(k)|$, it is natural to choose the value as large as possible. Thus, we set $\sum_{k\in\mathcal{S}} |\boldsymbol{\Delta}(k)| = \gamma\|\boldsymbol{\Delta}\|_1$ ($\gamma \lessapprox 1/2$). We then use the spark information as a prior to eliminate signal redundancy, thus improving signal processing efficiency. Notably, the computation of spark can be precomputed offline, avoiding extra complexity.

To sum up, the procedure is formalized in Algorithm 1. Lines 1 − 2 first describe the spark computation and influence, eliminating redundant iterations and identifying the sparse structures accurately. Lines 3 − 12 then describe the iterative process of bisection methods. Notably, line 6 specifies the support function and threshold to obtain the sparse structure. In terms of computational complexity, Algorithm 1 only costs $\mathcal{O}(N)$ flops since the bisection method has a linear complexity. Moreover, spark information further improve the iteration efficiency.

4.3. Sequential procedure

It is obvious that the solution (13) requires the inversion of a large-size matrix, which costs the computational complexity $\mathcal{O}(N^3)$. Therefore, we use the outer-product approximation to develop a computationally efficient procedure for approximating the inverse. First, we rewrite the outer-product approximation in matrix notation as

$$\boldsymbol{S}_t \triangleq \boldsymbol{A}^T\boldsymbol{A} + \boldsymbol{B}_t^T\boldsymbol{W}_t\boldsymbol{B}_t = \boldsymbol{A}^T\boldsymbol{A} + \sum_{i=1}^{t}(\omega_i\boldsymbol{s}_i\boldsymbol{s}_i^T). \tag{21}$$

Algorithm 1 Bisection method based on spark information.

Input: Given $\boldsymbol{A}$, γ, precision ϵ, the denser structural information $\mathcal{S}_0$ and the two local optimization solutions $\boldsymbol{x}_0, \boldsymbol{x}_1$. Assume $\|\boldsymbol{x}_0\|_0 > \|\boldsymbol{x}_1\|_0$, which indicates that $\boldsymbol{x}_1$ is a sparser representation than $\boldsymbol{x}_0$.
Output: The structural information $\mathcal{S}_1$.

Compute Spark($\boldsymbol{A}$) by solving $\mathcal{P}7$ and $\mathcal{P}8$ offline.
Initialize the structural information $\mathcal{S}_1 = \emptyset$, the upper bound $U =$ Spark($\boldsymbol{A}$), the low bound $L =$ Spark($\boldsymbol{A}$)/2.
Calculate the vector $\boldsymbol{\Delta} = \boldsymbol{x}_0 - \boldsymbol{x}_1$.
repeat
  Update $T = (U + L)/2$.
  Update $\mathcal{S}_1 = \text{supp}(|\boldsymbol{x}_1| > T)$.
  if $\sum_{k\in\mathcal{S}_1} |\boldsymbol{\Delta}(k)| < \gamma\|\boldsymbol{\Delta}\|_1$ **then**
    $U = T$,
  else
    $L = T$.
  end if
until $\left|\sum_{k\in\mathcal{S}_1} |\boldsymbol{\Delta}(k)| - \gamma\|\boldsymbol{\Delta}\|_1\right| < \epsilon$ or $|\mathcal{S}_1| \geq |\mathcal{S}_0|$.
return $\mathcal{S}_1 = \begin{cases} \mathcal{S}_0, & \text{if } |\mathcal{S}_1| \geq |\mathcal{S}_0|, \\ \mathcal{S}_1, & \text{otherwise.} \end{cases}$

Then, we derive a sequential procedure for building up the matrix $\boldsymbol{S}_t$ [31] by including local optimization points one at t^{th} iteration. Suppose we have already obtained the inverse $\boldsymbol{S}_t$ using the first t optimization points. By separating off the contribution from optimization point $t+1$, we obtain

$$\boldsymbol{S}_{t+1} = \boldsymbol{S}_t + \omega_t \boldsymbol{s}_t \boldsymbol{s}_t^T. \tag{22}$$

Taking the inverse from both sides, (22) can be written more compactly as follows

$$\left(\boldsymbol{S}_{t+1}\right)^{-1} = \left(\boldsymbol{S}_t\right)^{-1} - \frac{\left(\boldsymbol{S}_t\right)^{-1}\boldsymbol{s}_t\boldsymbol{s}_t^T\left(\boldsymbol{S}_t\right)^{-1}}{1/\omega_t + \boldsymbol{s}_t^T\left(\boldsymbol{S}_t\right)^{-1}\boldsymbol{s}_t}. \tag{23}$$

The initial matrix is defined as $\boldsymbol{S}_0 \triangleq \boldsymbol{A}^T\boldsymbol{A} + \alpha\boldsymbol{I}$, where α is a small quantity, and $(\boldsymbol{S}_0)^{-1}$ can be precomputed offline. Substituting (23) into (13) yields

$$\left(\boldsymbol{S}_{t+1}\right)^{-1}\boldsymbol{A}^T\boldsymbol{y} = \left(\boldsymbol{S}_t\right)^{-1}\boldsymbol{A}^T\boldsymbol{y} - \frac{\left(\boldsymbol{S}_t\right)^{-1}\boldsymbol{s}_t\boldsymbol{s}_t^T\left(\boldsymbol{S}_t\right)^{-1}}{1/\omega_t + \boldsymbol{s}_t^T\left(\boldsymbol{S}_t\right)^{-1}\boldsymbol{s}_t}\boldsymbol{A}^T\boldsymbol{y}, \tag{24}$$

$$\boldsymbol{x}_{t+1} = \boldsymbol{x}_t - \boldsymbol{h}_t\frac{c_t}{a_t + b_t}, \tag{25}$$

where $\boldsymbol{h}_t \triangleq \left(\boldsymbol{S}_t\right)^{-1}\boldsymbol{s}_t$, $c_t \triangleq \boldsymbol{s}_t^T\left(\boldsymbol{H}_t\right)^{-1}\boldsymbol{A}^T\boldsymbol{y}$, $b_t \triangleq \boldsymbol{s}_t^T\left(\boldsymbol{S}_t\right)^{-1}\boldsymbol{s}_t$ and $a_t \triangleq 1/\omega_t$.

4.4. Algorithm design

To sum up, Fig. 1 sketches the block diagram of the decorrelation IRLS algorithm. Also, the detailed steps are formalized in Algorithm 2. Lines 1 and 2 obtain the sparse signal initialization and the prior information spark by the means of ℓ_2-norm regulation and offline computation, respectively. Lines $4-11$ are the main steps of the decorrelation IRLS algorithm, as shown in the cycle module of Fig. 1. Specifically, lines $4-7$ update the sparsity vector, weighting factor, and optimization signal, respectively. Line 8 obtain the sparse structural information by invoking Algorithm 1. Line 9 describes the convergence condition of Algorithm 2, avoiding the redundant iterations by incorporating spark information.

The computational complexity of Algorithm 2 mainly comes from lines 6 and 7. Specifically, $\boldsymbol{A}^T\boldsymbol{y}$ is precomputed off-line, the parameters $\{a_t, b_t, c_t\}$ only cost $\mathcal{O}(1)$ flops. Therefore, the cost of Step 6 mainly comes from $\boldsymbol{h}_t\boldsymbol{h}_t^T$, it is approximately $\mathcal{O}(N^2/2)$. Moreover, Algorithm 2 further reduces the complexity by binary weights. The binary structure of weights minimizes the flops cost, enhancing the computational efficiency.

Algorithm 2 The decorrelation IRLS algorithm.

Input: Sampling vector $\boldsymbol{y} \in \mathbb{R}^M$, sensing matrix $\boldsymbol{A} \in \mathbb{R}^{M\times N}$, p, λ, regularization term ε, precision ε_s, β and the number of the maximal iterations τ.
Output: Practical solution $\boldsymbol{x}^*$.

1: Initialize $\left(\boldsymbol{S}_0\right)^{-1} = (\boldsymbol{A}^T\boldsymbol{A} + \alpha\boldsymbol{I})^{-1}$, $\boldsymbol{x}_1 = \left(\boldsymbol{S}_0\right)^{-1}\boldsymbol{A}^T\boldsymbol{y}$ and $\mathcal{S}_1 = \text{supp}(\boldsymbol{x}_1)$.
2: Compute Spark($\boldsymbol{A}$) by solving $\mathcal{P}7$ and $\mathcal{P}8$ offline.
3: **for** $t = 1, 2, \ldots, \tau$ **do**
4:   Update the vector $\boldsymbol{s}_t$ by (16).
5:   Update weight ω_t by (17).
6:   Update $\left(\boldsymbol{S}_t\right)^{-1}$ by using (23).
7:   Update $\boldsymbol{x}_{t+1}$ by using (25).
8:   Given $\mathcal{S}_t$, compute the structural information $\mathcal{S}_{t+1}$ by using Algorithm 1.
9:   **if** $|\mathcal{S}_{t+1}| \leq \lceil\beta\text{Spark}(\boldsymbol{A})\rceil$ or $\|\boldsymbol{x}_{t+1} - \boldsymbol{x}_t\|_2 \leq \varepsilon_s$ **then**
10:     Break.
11:   **end if**
12: **end for**

In the light of Theorem 2 in [29], we conclude that the proposed algorithm converges to an arbitrarily small value when α_0 is set to a sufficiently large value. After a sufficient number of iterations, the mean square error of the proposed algorithm becomes relatively small.

5. Simulation results and discussions

To verify the recovery accuracy of the proposed algorithm, the simulated signals $\boldsymbol{x}_0$ are generated by choosing k nonzero components uniformly out of $N = 1000$ and drawing the amplitude of each nonzero component from a uniform distribution of $U([-1, 1])$, where the sparsity level is $\mu = k/N$. The sensing matrix $\boldsymbol{A} \in \mathbb{R}^{M\times N}$ are i.i.d. Gaussian, with elements distributed $\mathcal{N}(0, 1/M)$, where M/N is the corresponding compressive ratio ρ. We generate random noise with i.i.d. $\mathcal{N}(0, \sigma^2)$ elements.

And then, we demonstrate spectrum sensing and power spectrum sensing with our proposed algorithm. We investigate the impact of several simulation parameters on the receiver operating characteristic (ROC) [12,16] of our detector. Here, we consider the simulated wideband signal $x(t) \in \mathcal{F} = [0, 320]$ MHz, namely, $x(t) = \sum_{i=1}^{k}\sqrt{E_i B_i}\text{sinc}\left(B_i\left(t - t_i\right)\right)e^{i2\pi f_i t} + n(t)$, where $\text{sinc}(x) = \sin(\pi x)/(\pi x)$, and E_i, t_i, f_i, respectively, represent the energy, the time offset and the central frequency of the i^{th} sub-band and $n(t)$ denotes the noise. The i^{th} sub-band covers the frequency range $\left[f_i - \frac{B_i}{2}, f_i + \frac{B_i}{2}\right]$.

5.1. Performance over the algorithm

In this simulation, we perform 500 Monto Carlo simulations in total. The acceptable reconstruction frequency $p = I/C$ is computed to evaluate the performance, where I, C denote the number of the successful reconstructions and simulations, respectively. We compare five algorithms, such as OMP [18], SOMP [20], IRLS [23], AR-IRLS [25], and the proposed algorithms, and also set the compression ratio ρ and sparsity level μ as reasonable ranges [0.05, 0.65] and [0.2, 0.8], respectively. The choices of compression ratios and sparse levels must meet the theoretical criteria $\rho = M/N \geq Ck\log(N/k)$ to calculate the minimum ρ for measurement matrix, where C denote constant [5,26].

Fig. 2 illustrates the convergence performance. As shown in Fig. 2(a), the bound of sparsity level gradually decreases with the increase of iterations and eventually converges to a fixed value Spark/2. This is because the designed structural information learning metrics facilitates the learning of sparsity, while the Spark/2 curve represents the lower bound of sparse solutions, characterizing the correlation information of the linear system. Fig. 2(b) shows that the proposed algorithm has the

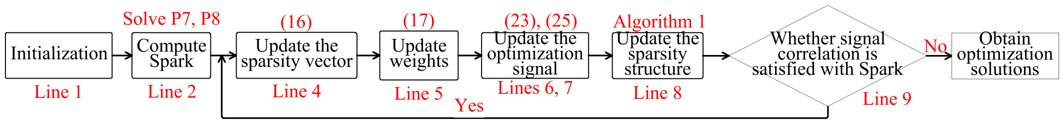

Fig. 1. The flowchart of Algorithm 2.

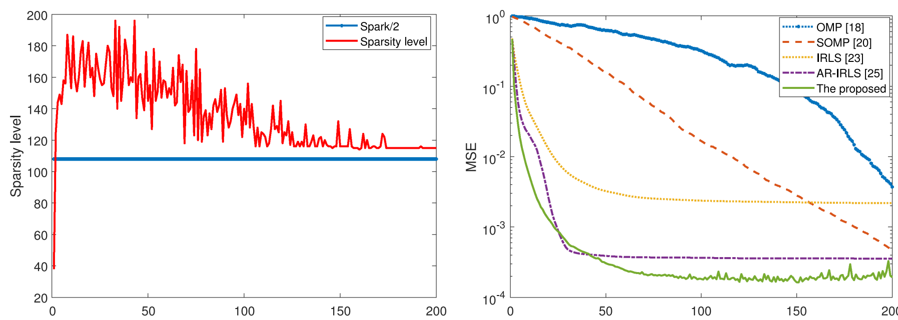

(a) Sparsity bound.

(b) Mean square error.

Fig. 2. Convergence performance.

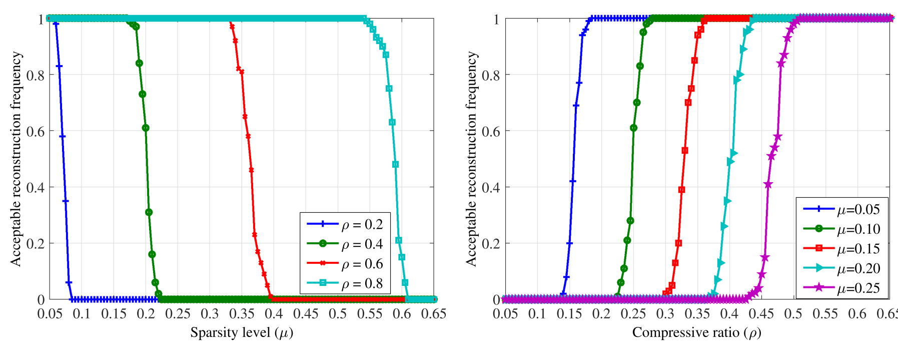

(a) Sparsity level μ.

(b) Compressive ratio ρ.

Fig. 3. Acceptable reconstruction frequency for the proposed algorithm.

fastest convergence speed and achieves the smallest MSE value. This is attributed to the sparse structure learning metric and Spark information verification, progressively ensuring decorrelation and obtaining the optimization sparse solution.

Fig. 3 presents the behavior of the acceptable reconstruction frequency. On the one hand, Fig. 3(a) shows that the reconstruction performance degrades as the sparsity level increases and the proposed algorithm can recover the signal even with a sparsity level μ beyond the 50 %, it is robust against the high sparsity levels. On the other hand, Fig. 3(b) shows that the reconstruction performance of the proposed algorithm improves as the compressive ratio increases. Additionally, the results indicate that the required sampling rate relies on the maximum sparsity level, which can be estimated through long-term spectral observations.

5.2. Spectrum detection

In this section, we investigate blind detection of both the power spectrum and the spectrum of a sparse signal. The number of potentially active transmissions is set to 3, and the number of signal samples is set to 1024, including all information of $x(t)$ [5,26]. The outer-product band of interest spans the range $[0, 320]$ MHz, divided into 64 channels of equal bandwidth $B = 5$ MHz [9,12]. Moreover, the settings of SNR $\in [-5\,\text{dB}, 10\,\text{dB}]$ and SR $\in [0.3, 0.5]$ are set to meet the noise power of Remark 1 and compressive ratio requirements, respectively.

To comprehensively evaluate the performance, we plot the ROC curves for our proposed method under different SNRs, as shown in Fig. 4. It is evident that our method achieves reliable detection performance up to a certain SNR threshold, below which the performance degrades rapidly. Additionally, we observe a distinct critical point in the ROC curves when the SNR is greater than or equal to 5 dB. To the left of this critical point, the probability of detection increases rapidly with the probability of false alarm. In contrast, to the right of this point, the probability of detection increases at a significantly slower rate. These results demonstrate the robustness of our proposed method in noisy environments.

Next, we evaluate the performance of our proposed method under different sampling rates (SR), which are related to the number of measurements. The sampling parameters are configured as described above, and SNR is set to 10 dB. As illustrated in Fig. 5, our method requires a minimum number of samples to achieve satisfactory detection performance. Specifically, when the sampling rate exceeds 0.375, the performance improvement becomes marginal, whereas below this threshold, the performance degrades significantly. These results demonstrate that our proposed method is robust for outer-product band signals even at low sampling rates.

Fig. 6 compares our algorithm with others, including different optimization algorithms and spectrum sensing architectures. Fig. 6(a) shows that when the probability of false alarm is 0.2, the probability of detection of the proposed reaches approximately 0.98, followed by IRLS (i.e., 0.95), OMP (i.e., 0.92), and AR-IRLS (i.e., 0.9), given SNR = 10 dB and SR = 0.375. Consistent results are obtained with SNR = 5 dB. Evidently, our detector outperforms other algorithms given the same SNR and SR.

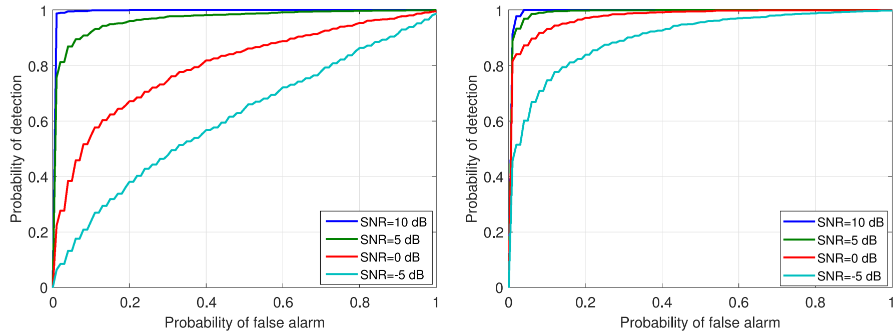

(a) The ROC with spectrum sensing versus SNR. (b) The ROC with power spectrum sensing versus SNR.

Fig. 4. Influence of the SNR on the ROC.

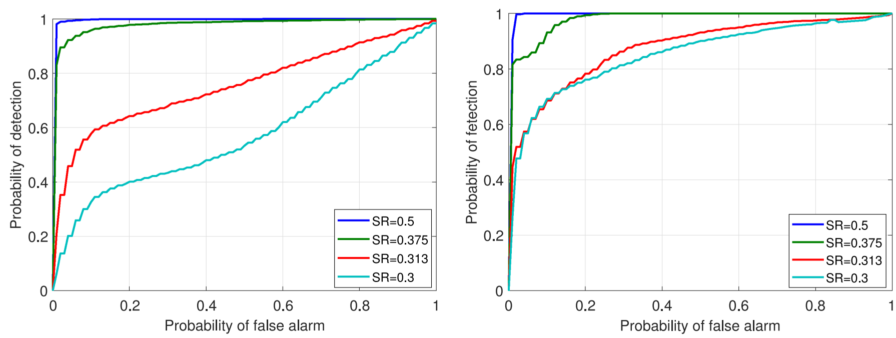

(a) The ROC with spectrum sensing versus SR. (b) The ROC with power spectrum sensing versus SR.

Fig. 5. Influence of the sampling rate on the ROC. Here, given SNR = 10dB.

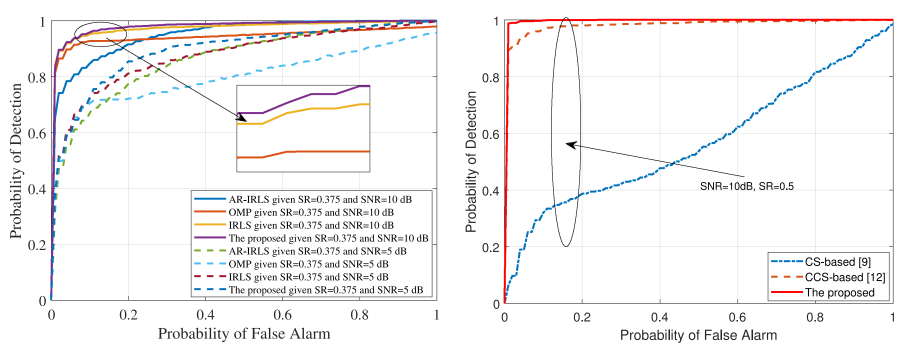

(a) Different optimization algorithms. (b) Different sensing architectures.

Fig. 6. The ROC with spectrum sensing.

Since the structure-promoting matrices store the sparsity information of spectrum sensing, the proposed method achieves the optimization point with higher probability. On the other hand, Fig. 6(b) also shows our proposed algorithm outperforms conventional CSS-based and CCS-based algorithms. It is also due to structure-promoting matrices, employing adaptive learning for environmental information.

6. Conclusions

This paper has proposed a decorrelation spectrum sensing model with structural information learning. To address this problem, a sparsity bound and spark were developed to learn the structural information. An accelerated iterative re-weighted least-squares algorithm was designed to control computational complexity and achieve real-time spectrum sensing. Numerical experiments demonstrated that the proposed achieves faster convergence speed and higher reconstruction precision with few measurements and high sparsity levels, enabling excellent performance in spectrum sensing applications. Future work includes extending the proposed algorithm to real-world signal scenarios, i.e., National Instruments USRP E320.

Data availability

No data was used for the research described in the article.

Declaration of competing interest

Shuwu Chen reports financial support was provided by Project of Industry-university-institute Cooperation in Colleges and Universities in Fujian Province, Fujian Provincial Department of Science and Technology. Shuwu Chen reports financial support was provided by Project of Industry-university-institute Joint Innovation in Colleges and Universities in Fujian Province, Fujian Provincial Department of Science and Technology. Haihui Xie reports a relationship with Project of Industry-university-institute Cooperation in Colleges and Universities in Fujian Province that includes: board membership and employment. If there are

other authors, they declare that they have no known competing financial interests or personal relationships that could have appeared to influence the work reported in this paper.

Appendix A. Proof of Lemma 1

Here, to derive the optimization problem $\mathcal{P}6$, we define a set of alternative solutions as follows around $\boldsymbol{x}_1$

$$\mathcal{C} \triangleq \left\{ (\boldsymbol{\Delta}, \mathcal{S}_1) \middle| \|\boldsymbol{x}_1 + \boldsymbol{\Delta}\|_1 - \|\boldsymbol{x}_1\|_1 \geq 0, \boldsymbol{A\Delta} = \boldsymbol{0}, \mathcal{S}_1 = \mathrm{supp}(\boldsymbol{x}_1) \right\},$$

where $\boldsymbol{\Delta} \triangleq \boldsymbol{x}_0 - \boldsymbol{x}_1$. The strategy of the proof we are about to present is to enlarge this set.

Writing the difference in norms as a difference in sums and relabeling the summations give the formalization as follows.

$$\begin{aligned} \|\boldsymbol{x}_0\|_1 - \|\boldsymbol{x}_1\|_1 &= \sum_{k\in\mathcal{S}_1^c} |\boldsymbol{x}_0(k)| + \sum_{k\in\mathcal{S}_1} \left(|\boldsymbol{x}_0(k)| - |\boldsymbol{x}_1(k)|\right) \\ &\geq \sum_{k\in\mathcal{S}_1^c} |\boldsymbol{x}_0(k)| - \sum_{k\in\mathcal{S}_1} |\boldsymbol{x}_0(k) - \boldsymbol{x}_1(k)| \qquad (26a) \\ &= \sum_{k\in\mathcal{S}_1^c} |\boldsymbol{\Delta}(k)| - \sum_{k\in\mathcal{S}_1} |\boldsymbol{\Delta}(k)|, \qquad (26b) \end{aligned}$$

where (26a) is obtained by the inequality $|a+b| - |b| \geq -|a|$. Combining (26b) with the above condition, we can relax the condition $\|\boldsymbol{x}_0\|_1 - \|\boldsymbol{x}_1\|_1 \geq 0$ instead

$$0 \leq \sum_{k\in\mathcal{S}_1^c} |\boldsymbol{\Delta}(k)| - \sum_{k\in\mathcal{S}_1} |\boldsymbol{\Delta}(k)| \leq \|\boldsymbol{x}_0\|_1 - \|\boldsymbol{x}_1\|_1. \qquad (27)$$

This inequality (27) can be written more compactly by adding and subtracting the term $\sum_{\mathcal{S}_1} |\boldsymbol{\Delta}(k)|$, this leads to

$$\sum_{k\in\mathcal{S}_1} |\boldsymbol{\Delta}(k)| \leq \frac{1}{2}\|\boldsymbol{\Delta}\|_1.$$

Thus, substituting into the set $\mathcal{C}$, this leads to

$$\mathcal{C} \subseteq \mathcal{C}^1 \triangleq \left\{ (\boldsymbol{\Delta}, \mathcal{S}_1) \middle| \sum_{k\in\mathcal{S}_1} |\boldsymbol{\Delta}(k)| \leq \frac{1}{2}\|\boldsymbol{\Delta}\|_1, \boldsymbol{A\Delta} = \boldsymbol{0}, \mathcal{S}_1 = \mathrm{supp}(\boldsymbol{x}_1) \right\}.$$

We now turn to handle the requirement $\mathcal{S}_1 = \mathrm{supp}(\boldsymbol{x}_1)$, replacing it with a relaxed requirement $\mathrm{supp}(\boldsymbol{x}_1) \subseteq \mathcal{S} \subseteq \mathrm{supp}(\boldsymbol{x}_0)$ that expands the set $\mathcal{C}^1$ further as follows

$$\mathcal{C}^1 \subseteq \left\{ (\boldsymbol{\Delta}, \mathcal{S}) \middle| \sum_{k\in\mathcal{S}} |\boldsymbol{\Delta}(k)| \leq \frac{1}{2}\|\boldsymbol{\Delta}\|_1,\ \boldsymbol{A\Delta} = \boldsymbol{0},\ \mathrm{supp}(\boldsymbol{x}_1) \subseteq \mathcal{S} \subseteq \mathrm{supp}(\boldsymbol{x}_0) \right\}.$$

The enlargement will be done so as to simplify $\mathcal{P}5$, up to the sparser representation where the sparer structural information $\mathcal{S}$ can be assessed by $\mathcal{P}6$.

CRediT authorship contribution statement

Haihui Xie: Conceptualization, Methodology, Software, Writing - original draft; **Shuwu Chen:** Supervision, Project administration, Funding acquisition; **Zhaogang Shu:** Formal analysis, Validation, Writing - review & editing; **Fangqing Tan:** Investigation, Data curation, Visualization.

Reference

[1] A. Gharib, W. Ejaz, M. Ibnkahla, Distributed spectrum sensing for IoT networks: architecture, challenges, and learning, IEEE Internet Things Mag. 4 (2) (2021) 66–73.

[2] T. Jiang, M. Jin, Q. Guo, J. Yao, Graph learning-based cooperative spectrum sensing with corrupted RSSs in spectrum-heterogeneous cognitive radio networks, IEEE Trans. Wireless Commun. 23 (10) (2024) 15447–15461.

[3] G. Zhu, J. Wu, H. Liang, J. Tang, L. Xia, J. Bao, W. Cao, Cost and benefit tradeoff of SSDF attack in cooperative spectrum sensing in cognitive wireless sensor networks, IEEE Sensors Lett. 8 (5) (2024) 1–4.

[4] E.J. Candes, J. Romberg, T. Tao, Robust uncertainty principles: exact signal reconstruction from highly incomplete frequency information, IEEE Trans. Inf. Theory 52 (2) (2006) 489–509. https://doi.org/10.1109/TIT.2005.862083

[5] C. Zhou, Y. Gu, Z. Shi, M. Haardt, Structured nyquist correlation reconstruction for DOA estimation with sparse arrays, IEEE Trans. Signal Process. 71 (11) (2023) 1849–1862.

[6] D. Liu, Y. Zhao, T. Zhang, Sparsity-based two-dimensional DOA estimation for coprime planar array via enhanced matrix completion, Remote. Sens. 14 (19) (2022) 4690.

[7] S. Jiang, N. Fu, Z. Wei, X. Li, L. Qiao, X. Peng, Joint spectrum, carrier, and DOA estimation with beamforming MWC sampling system, IEEE Trans. Instrum. Meas. 71 (3) (2022) 1–15.

[8] L. Guo, C. Kok, H.C. So, W. Tam, Dual-band signal reconstruction based on periodic nonuniform sampling at optimal sampling rate, Digit. Signal Process. 120 (2022) 103252.

[9] L. Yang, H. Ma, H. Tang, J. Wang, R. Qin, Improved-SOMP algorithm based on principal component estimation for wideband spectrum sensing, IEEE Trans. Veh. Technol. 74 (6) (2025) 9932–9937.

[10] S. Wen, P. Wang, W. Jiang, M. Li, A mixing sequence optimization method for focused compressed sampling based on modulated wideband converter, IEEE Trans. Circuits Syst. II Express Briefs 69 (12) (2022) 4704–4708.

[11] K. Chae, J. Park, Y. Kim, Rethinking autocorrelation for deep spectrum sensing in cognitive radio networks, IEEE Internet Things J. 10 (1) (2023) 31–41.

[12] J. Liu, X.-L. Huang, F. Hu, C. Li, Adaptive compressive spectrum sensing using a deterministic estimation model for wideband cognitive radios, IEEE Trans. Wireless Commun. 2 (14) (2025) 155–168.

[13] L. Liu, Z. Zhang, X. Zhang, P. Wei, J. An, H. Li, Joint spectrum sensing and DOA estimation based on a resource-efficient sub-nyquist array receiver, IEEE Trans. Signal Process. 72 (12) (2024) 5354–5370.

[14] L. Yang, J. Fang, H. Duan, H. Li, Fast compressed power spectrum estimation: toward a practical solution for wideband spectrum sensing, IEEE Trans. Wireless Commun. 19 (1) (2020) 520–532.

[15] S. Liu, L. Zhao, S. Li, A novel all-digital calibration method for timing mismatch in time-interleaved ADC based on modulation matrix, IEEE Trans. Circuits Syst. I Regul. Pap. 69 (7) (2022) 2955–2967.

[16] K. Jiang, D. Wang, K. Tian, H.C. Feng, Y.X. Zhao, S. Cao, J. Gao, X. Zhang, Y. Li, J. Yuan, Y. Xiong, B. Tang, Wideband power spectrum sensing: a fast practical solution for nyquist folding receiver, IEEE Internet Things J. 11 (13) (2024) 24098–24108.

[17] R. Konda, R. Chandan, D. Grimsman, J.R. Marden, Optimal utility design of greedy algorithms in resource allocation games, IEEE Trans. Automatic Control 69 (10) (2024) 6592–6604.

[18] L. Lu, W. Xu, Y. Wang, Z. Tian, Blind orthogonal least squares based compressive spectrum sensing, IEEE Trans. Veh. Technol. 72 (12) (2023) 16772–16776.

[19] J. Kim, J. Wang, L.T. Nguyen, B. Shim, Joint sparse recovery using signal space matching pursuit, IEEE Trans. Inf. Theory 66 (8) (2020) 5072–5096.

[20] N. Han, S. Li, J. Lu, Orthogonal subspace based fast iterative thresholding algorithms for joint sparsity recovery, IEEE Signal Process. Lett. 28 (3) (2021) 1320–1324.

[21] J. Kim, J. Wang, B. Shim, Optimal restricted isometry condition of normalized sampling matrices for exact sparse recovery with orthogonal least squares, IEEE Trans. Signal Process. 69 (17) (2021) 1521–1536.

[22] B. Zheng, C. Zeng, S. Li, G. Liao, Recovery guarantee analyses of joint sparse recovery via tail $\ell_{2,1}$ minimization, IEEE Trans. Signal Process. 71 (10) (2023) 4342–4352.

[23] A. Wan, Uniform RIP conditions for recovery of sparse signals by ℓ_p $(0 < p \leq 1)$ minimization, IEEE Trans. Signal Process. 68 (3) (2020) 5379–5394.

[24] W. Xiong, C. Schindelhauer, H.C. So, S.J. Rupitsch, A message passing based iterative algorithm for robust TOA positioning in impulsive noise, IEEE Trans. Veh. Technol. 72 (1) (2023) 1048–1057.

[25] X. Zhang, Y. Ma, Y. Gao, S. Cui, Real-time adaptively regularized compressive sensing in cognitive radio networks, IEEE Trans. Veh. Technol. 67 (2) (2018) 1146–1157. https://doi.org/10.1109/TVT.2017.2749254

[26] H. Ma, X. Yuan, L. Zhou, B. Li, R. Qin, Joint block support recovery for sub-nyquist sampling cooperative spectrum sensing, IEEE Wireless Commun. Lett. 12 (1) (2023) 85–88.

[27] I. Bisio, C. Garibotto, A. Grattarola, F. Lavagetto, A. Sciarrone, M. Zerbino, SHM With low-cost, low-energy, and low-rate IoT devices: reducing transmission burden with compressive sensing, IEEE Internet Things J. 11 (13) (2024) 24323–24333.

[28] M. Elad, Sparse and Redundant Representations-from Theory to Applications in Signal and Image Processing, Springer Publishing Company, 2010.

[29] H. Xie, P. Wu, F. Tan, M. Xia, Adaptively-regularized compressive sensing with sparsity bound learning, IEEE Commun. Lett. 25 (4) (2021) 1283–1287.

[30] D.A. Guimaraes, G.H.F. Floriano, L.S. Chaves, A tutorial on the CVX system for modeling and solving convex optimization problems, IEEE Lat. Am. Trans. 13 (5) (2015) 1228–1257. https://doi.org/10.1109/TLA.2015.7111976

[31] C.M. Bishop, Pattern Recognition and Machine Learning (Information Science and Statistics), Springer-Verlag New York, Inc., 2006.